International Journal of Thermal Sciences 109 (2016) 413–423

Contents lists available at ScienceDirect

International Journal of Thermal Sciences

journal homepage: www.elsevier.com/locate/ijts

Corrections for lateral conduction error in steady state heat transfer measurements

D. Sarkar [a], A. Jain [a], R.J. Goldstein [b], V. Srinivasan [b, *]

[a] Department of Mechanical and Aerospace Engineering, The University of Texas at Arlington, Arlington, TX 76019, USA
[b] Department of Mechanical Engineering, University of Minnesota, Minneapolis, MN 55455, USA

ARTICLE INFO

Article history:
Received 24 December 2015
Received in revised form
27 May 2016
Accepted 28 May 2016

Keywords:
Lateral conduction error
Heat transfer correction
Analytical thermal conduction modeling
Spatially varying convective heat transfer
Jet impingement

ABSTRACT

Steady state measurements of convective heat transfer coefficient often use a constant wall heat flux condition along with measured temperature distribution to generate heat transfer coefficient maps. Large spatial gradients in the heat transfer coefficient may lead to lateral conduction within the heater foil, causing non-uniformity in the actual convective flux into the fluid, yielding errors in the calculated Nusselt numbers. This paper presents an analytical procedure for correcting such errors for a model system with a known heat transfer coefficient distribution and nominal 1-D applied wall heat flux. The resulting 2-D conduction problem is parametrized in terms of the Biot number *Bi* and the heat transfer coefficient distribution, expressed by the change in magnitude ρ and the peak gradient γ, as well as the proximity of the gradient region to a symmetry plane. Three model configurations are studied: a region of large gradients that is located far away from lateral boundaries, and two cases where the gradient region is located near a symmetry plane, viz. impingement heat transfer due to a slot jet and a round jet. It is shown that sharp spatial variations in heat transfer coefficient can lead to significant error in Nusselt number determination when the wall heat flux is assumed to be uniform. The error is shown to be amplified when the gradient region is located near a symmetry plane. Finally, the wall heat flux is correlated using of an expression that captures the results of the analytical calculations for the ranges of Bi, ρ and γ studied, which can be used to evaluate experimental designs for heat transfer measurement, and make corrections for the two-dimensional nature of heat transfer in the foil and insulation.

1. Introduction

The trend of increasing inlet temperatures in gas turbines and the corresponding high cooling requirements of turbine blades requires the development of novel cooling schemes. Accurate measurements that characterize the performance of these cooling schemes are critical for reliable design. In order to estimate the true operating temperatures of various hot section components, designers rely on heat transfer coefficient data obtained from low-temperature tests. Small errors in measurements of the heat transfer coefficient can lead to moderate uncertainties in metal operating temperature, and large uncertainties in blade lifetime prediction [1]. Despite considerable care taken by researchers, it is well known that uncertainties in heat transfer experiments are rarely less than 8–10%. Several techniques are currently used for the measurement of heat transfer coefficients in lab-scale experiments. In recent years, thermocouple-based measurements of temperature at discrete spatial locations have almost completely given way to high resolution whole surface measurements utilizing Thermochromic Liquid Crystals (TLCs), Infra-Red Thermography (IRT), Temperature Sensitive Paint (TSP) or Pressure Sensitive Paint (PSP). All of these techniques, when carefully calibrated, enable temperature measurements with high spatial resolution and low measurement uncertainty of the order of 0.5 K [2].

Independent of the temperature measurement technique, there are mainly two methods for measurement of heat transfer coefficient on a surface, given by the thermal boundary condition on the surface. Steady-state measurements typically use a constant heat flux surface, established by thin metal foil heaters. The local heat transfer coefficient is found by the relation, $h(\vec{r}) = q_w/(T_w(\vec{r}) - T_\infty)$ where q_w is the convective heat flux into the fluid after subtracting losses from the power input. The heat loss can be minimized by insulating the heater foil from the back, i.e. on the side not exposed to the flow, and by minimizing radiation

* Corresponding author.
E-mail address: vinods@umn.edu (V. Srinivasan).

http://dx.doi.org/10.1016/j.ijthermalsci.2016.05.031
1290-0729/

Nomenclature:

a	width, (m)
b	thickness, (m)
g	volumetric heat generation rate, (W/m^3)
h_{min}	minimum convective heat transfer coefficient, (W/m^2-K)
h_{max}	maximum convective heat transfer coefficient, (W/m^2-K)
k	thermal conductivity, (W/m-K)
$\tilde{q}_c$	heat flux correction factor, Section 2.3
r	radial coordinate, (m)
x	cartesian coordinate, (m)
y	cartesian coordinate, (m)
z	axial coordinate, (m)
Bi	Biot number, ($h_{max}\ b_2/k_2$)
N	maximum number of eigenvalues
T	temperature, (K)

Greek:

β	thickness ratio (b_1/b_2)
γ	gradient parameter
λ	eigenvalue, (m^{-1})
κ	ratio of thermal conductivities (k_2/k_1)
ρ	ratio of heat transfer coefficients (h_{max}/h_{min})

Subscripts:

1	insulation
2	foil

loss, which may not always be possible. The uncertainty in estimation of the lost power input can be reduced by having a good knowledge of the emissivity of the foil material, and the thermal properties of the insulation.

Transient experiments utilize the assumption of one-dimensional conduction into a semi-infinite medium in order to reconstruct the heat transfer coefficient. The surface temperature field is measured at two different times, and the data are plugged into an analytical solution to extract the heat transfer coefficient. This method and its several variations have been extended for simultaneous calculation of heat transfer coefficient and cooling effectiveness in film cooling flows [3]. Mass transfer based measurements, such as the naphthalene sublimation technique [4], measure transport coefficient distributions over a sublimating surface. Using the analogy between heat and mass transfer in boundary layer flows, these mass transfer distributions can be converted to heat transfer coefficient distributions.

Each of these techniques have distinct advantages and disadvantages. Steady-state measurements are conceptually simple and are easy to set up. When used with TLCs, the technique is inexpensive but time-consuming. The transient IR technique is often preferred nowadays, but requires greater care in calibration of the IR camera [5]. Both these techniques suffer from the deficiency that a 1-D conduction model is assumed for the heat flux in one instance, and for the thermal penetration in the other. As such, both methods are unreliable in regions of strong lateral variation of heat transfer coefficient or geometry. The mass transfer technique based on naphthalene sublimation avoids many of these issues. This technique implicitly simulates a constant temperature boundary condition, and is not subject to lateral conduction error. This technique is capable of very high spatial resolution, and the conversion from mass transfer coefficients (Sherwood numbers) to heat transfer coefficients (Nusselt numbers) has been shown to be reliable in complex systems such as endwall secondary flows [6]; however, it has not been fully established for regions with recirculating flows, such as immediately downstream of film holes or backward facing steps, or in regions where erosion may cause mass transfer, such as stagnation points of impinging jets.

In this paper, we focus on the lateral conduction error introduced in steady state heat transfer measurements. Lateral conduction errors arise when a constant wall flux is assumed in the presence of large gradients in heat transfer coefficient. If the flux in the heater were purely normal to the surface, these gradients in heat transfer coefficient would cause large gradients in wall temperature. As a result, the path of least thermal resistance from below a low-heat transfer region may involve lateral conduction along the foil into the region of high heat transfer. Such lateral conduction within the foil leads to a non-uniform wall-normal heat flux distribution, which needs to be accounted for during the data reduction process.

For the transient heat transfer technique utilizing the assumption of conduction into a semi-infinite medium, the effects of lateral conduction have been documented and analyzed. An early study was by Vedula and Metzger [7], who performed numerical simulations to quantify the effect of lateral conduction, including the effect of anisotropic conduction. Lin and Wang [8] used an inverse 3-D algorithm to avoid making the 1-D heat transfer approximation when processing the raw hue data. They attribute the 12% difference between their results and the results of the 1-D procedure to the effect of lateral conduction. Kingsley-Rowe et al. [9] used a modified version of the 1-D analytical solution and applied a Biot number correction in order to calculate the heat transfer coefficient in the presence of lateral conduction. Bons [10] applied a finite volume method to study the effect of lateral conduction in the presence of surface roughness and showed that the 1-D model is inadequate for rough surfaces, due to large peak-to-valley variation in heat transfer coefficients. A comprehensive model for the effects of flow temperature variation and heater foil response in conjunction with lateral conduction on the measurement uncertainty has been presented by von Wolfersdorf and co-workers [11,12].

These studies confirm that the effects of lateral conduction are most pronounced when there are sharp gradients in the heat transfer coefficient. Such sharp gradients exist at several locations on a modern gas turbine blade, such as the point of laminar/turbulent transition, stagnation points on blade leading edge, as well as on internal channels cooled by showerhead film holes, and separation/reattachment regions near tip/hub endwalls. As an example, consider the distribution of transport coefficient along the blade suction surface shown in Fig. 1 for a representative high-performance blade profile [13]. Starting from its peak near the leading edge stagnation point, the Sherwood number drops by a factor of 4 over a streamwise distance of 10% of blade chord. Similarly, near the trailing edge, the Sherwood number rises by a factor of 6 over a streamwise distance of 20% of the blade chord, due to laminar-turbulent transition. Such sharp gradients can occur in a region where the upstream and downstream transport coefficients are relatively uniform (as for Tu = 18% in the figure) or near a point of nominal symmetry, such as the leading edge.

While the effect of lateral conduction has been well investigated

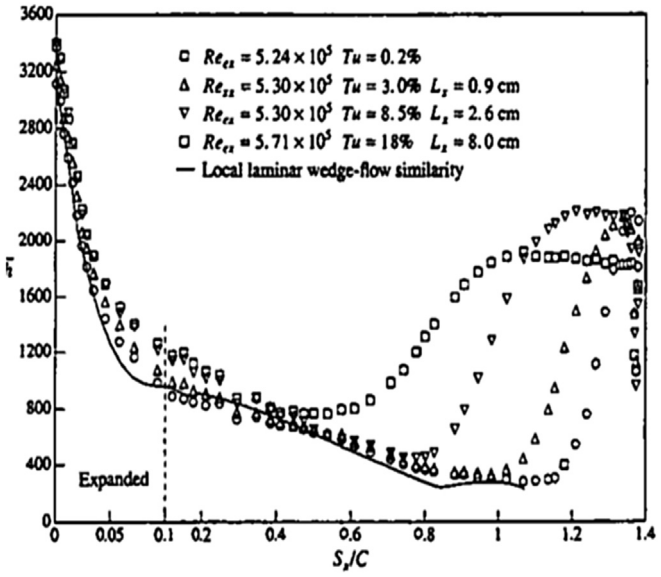

Fig. 1. Midspan Sherwood number distribution on the suction surface of a high performance turbine rotor blade (reproduced with permission from Wang et al., 1998, [13]).

for the transient measurement technique, little information is available on the appropriate correction for the steady state technique. The steady state technique continues to be used by several groups for gas turbine heat transfer [14,15]. Partly, this is because a quick estimate for the lateral conduction correction can be obtained by taking the Laplacian of the observed temperature field on the surface, and adding/subtracting that to the nominal heat flux [16]. However, as we will show, the exact error is sensitive to the location of the gradient region and the behavior of the heat transfer coefficient profile on either side of the gradient region. In this paper, we outline a technique to estimate *a priori* the error due to the assumption of a uniform wall heat flux in a steady state heat transfer experiment.

The rest of this paper is organized as follows: Section 2 presents the mathematical framework used to analyze the two-dimensional conduction problem. Briefly, it involves expansion of the unknown temperature field in terms of orthogonal functions (Fourier series) and applying the boundary conditions to evaluate the unknown coefficients. Section 2.1 discusses the problem of a slot jet for two cases, one when the jet width is much larger than the gradient region, and another when it is comparable. Section 2.2 repeats the analysis for a circular jet. Section 2.3 defines a heat flux correction factor, which can be applied to nominal 1-D calculations in order to account for two-dimensional effects. Section 3 presents the results of the calculations, as well as correlations for the correction factor. Section 4 summarizes the conclusions of this study.

2. Mathematical modeling

A typical test section for studying heat transfer to a jet from a constant-flux involves the use of a resistive foil of thickness b_2 (typically 50 μm) stretched over an insulating surface, as is shown in Fig. 2. The insulation is usually a low conductivity polymer, with or without an air gap to further increase the thermal resistance beneath the foil. The present mathematical analysis can include variation in the fluid jet temperature, for example compressible jets and film cooling applications. If one accounts for such variations in the estimation of local heat transfer distribution, the analytical procedure illustrated here is well suited to estimate the error in the heat transfer distribution due to lateral conduction. The thickness b_1 of the insulation is chosen such that even for low values of the heat transfer coefficient, the thermal resistance in the downward direction (b_1/k_1) is much greater than the thermal resistance above the foil ($1/h_{min}$). The thermal conductivities of the insulation and foil are given by k_1 and k_2. The convective heat transfer coefficient on the top surface is assumed to vary spatially, $h = h(x)$ or $h(r)$, as is the case with slot and radial jets.

To obtain the local wall heat flux at every location, we solve for the temperature distribution in a two-layer medium with heat generation in the top layer, which is convectively cooled. Using the temperature solution in the multilayer body, an expression for the heat flux correction factor is determined to account for the effect of lateral conduction. The mathematical model discussed in this section assumes thermal conduction in the insulation material to be anisotropic, as is often the case. Heat transfer in the case of isotropic materials is discussed as a special case. The error estimated by the correction factor results in quantification of the lateral conduction effects within the foil in regions of sharp gradient of convective heat transfer.

In order to understand the effects of gradient in heat transfer coefficient, we choose an idealized distribution which is parametrized in terms of its maximum and minimum values, as well as the region over which this variation occurs, expressed in terms of the maximum slope. For the case of a gradient region that is far away from any boundaries (such as the transition region in Fig. 1 and laminar and turbulent components of an air jet over a circular disk [17]), we use the expression

$$\frac{h(x)}{h_{max}} = \frac{1 - R\tanh\left(\gamma\left(\frac{x-10}{w}\right)\right)}{(1+R)} \tag{1}$$

where $\rho = h_{max}/h_{min}$ and $R = (\rho - 1)/(\rho + 1)$. The parameter γ is directly proportional to the maximum slope in the heat transfer coefficient, and inversely proportional to the region over which the variation occurs. The parameter w, corresponds to the width of the gradient region for the case of an asymmetric jet and jet-half width for the case of a symmetric jet.

This expression is plotted in Fig. 3 for $\rho = 5$, and various values of γ. The function asymptotes to 1 at $x/w = 5$ and to 0.2 at $x/w = 15$ where x/w is in the range of 0–20. The steepness of the gradient is characterized by the gradient parameter γ, and is centered at $x/w = 10$.

For the case corresponding to a slot/plane jet, we use the distribution to represent the case of an impingement region where the gradient region is centered on 1, adjacent to a symmetry plane. The expression is given by $h(x) = h_{max}\left(1 + R\tanh\left(\gamma\left(\frac{w}{x} - \frac{x}{w}\right)\right)\right)\Big/(1+R)$. From observation, when $x \to 0$, $\tanh\left(\gamma\left(\frac{w}{x} - \frac{x}{w}\right)\right) \approx 1$. As a result, in the above equation, $h(x)$ reduces to h_{max} as $x \to 0$. A similar expression in radial co-ordinates is used in calculations for a round jet in which the spatial co-ordinate x in above equations for $h(x)$ is replaced by the radial co-ordinate r.

2.1. Heat transfer due to a slot jet

The geometry of the slot jet case is shown in Fig. 2(b). Note that while the heater foil (layer 2), typically a metal, is usually isotropic ($k_{2x} = k_{2y} = k_2$), thermal conduction in the insulation layer, typically a low thermal conductivity material, may be orthotropic ($k_{1x} \neq k_{1y}$).

The following parameters are used for non-dimensionalization of this problem:

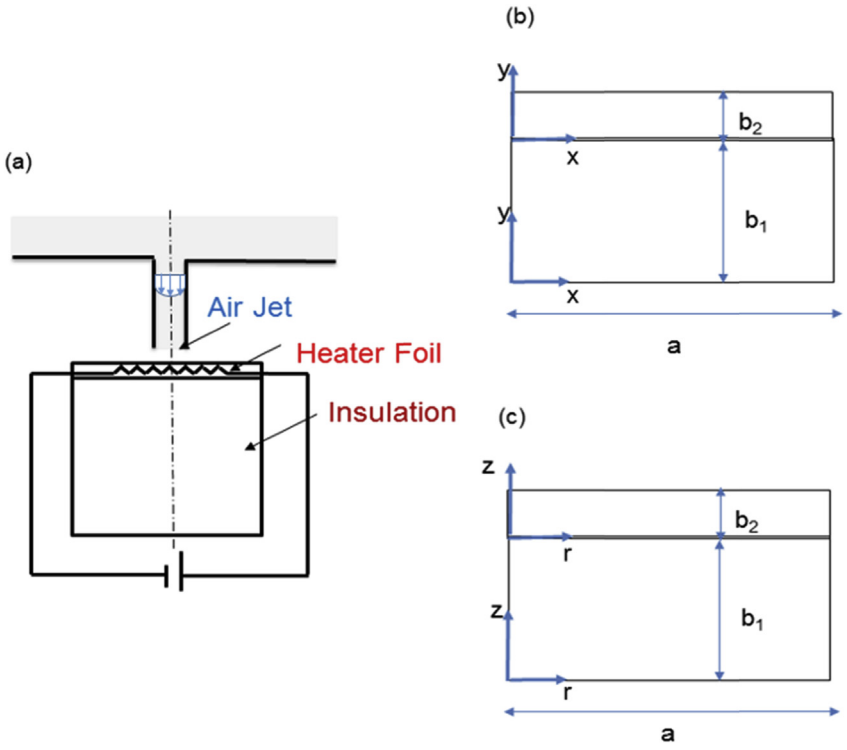

Fig. 2. (a) Schematic of the experimental setup for jet impingement cooling of a metal foil with an insulation layer, (b) Geometry for slot jet cooling in cartesian coordinates, (c) Geometry for circular jet cooling in cylindrical coordinates.

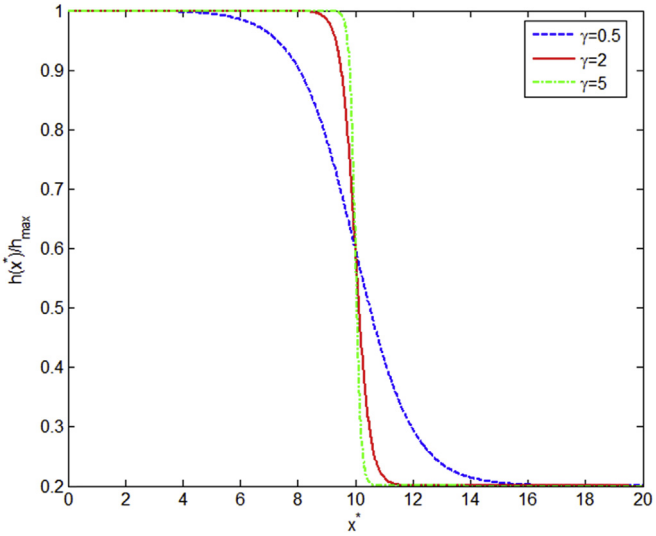

Fig. 3. Heat transfer coefficient as a function of x for different values of γ.

$$x^* = \frac{x}{w};\ y^* = \frac{y}{w};$$
$$a^* = \frac{a}{w};\ b_1^* = \frac{b_1}{w};\ b_2^* = \frac{b_2}{w};$$
$$T_j^* = \frac{k_2\ (T_j - T_\infty)}{g_2\ w^2};$$
$$Bi = \frac{h_{\max} b_2}{k_2};\ \psi_j = \begin{cases} 0 & j = 1 \\ 1 & j = 2 \end{cases} \quad (2)$$

For convenience, the star (*) notation is dropped in the remainder of this paper, so that all subsequent variables are in dimensionless form. The governing energy conservation equation is given by

$$\frac{\partial^2 T_j}{\partial x^2} + \left(\frac{k_{j,y}}{k_{j,x}}\right) \frac{\partial^2 T_j}{\partial y^2} + \frac{k_2\ \psi_j}{k_{j,x}} = 0 \quad \text{for j} = 1,\ 2 \quad (3)$$

where heat generation occurs only in the metal foil layer due to Joule heating. It must also be noted that the heat generation in the foil due to Joule heating is assumed to be uniform. This is usually achieved by choosing a material with low temperature coefficient of resistance. This equation is subject to the following boundary conditions and interface conditions

$$T_1(x, 0) = 0 \quad (4)$$

$$\left.\frac{\partial T_2}{\partial y}\right|_{y=b_2} + \frac{Bi}{b_2} h(x)\ T_2(x, b_2) = 0 \quad (5)$$

$$\left.\frac{\partial T_j}{\partial x}\right|_{x=0,a} = 0 \quad \text{for } j = 1,\ 2 \quad (6)$$

$$T_1(x, b_1) = T_2(x, 0) \quad (7)$$

$$k_{1,y} \left.\frac{\partial T_1}{\partial y}\right|_{y=b_1} = k_2 \left.\frac{\partial T_2}{\partial y}\right|_{y=0} \quad (8)$$

Equations (7) and (8) represent the compatibility condition at the interface where each layer is assigned its individual co-ordinate system with the origin at the bottom-left corner of each layer. The following transformation absorbs the non-homogeneity from the governing Equation (3):

$$T_j(x,y) = \theta_j(x,y) - \left(\frac{k_2}{k_{j,x}}\right)\frac{\psi_j}{2}y^2 \tag{9}$$

Based on the above transformation the transformed boundary value problem is given by

$$\frac{\partial^2\theta_j}{\partial x^2} + \left(\frac{k_{j,y}}{k_{j,x}}\right)\frac{\partial^2\theta_j}{\partial y^2} = 0 \tag{10}$$

subject to the following boundary conditions and interface conditions

$$\theta_1(x,0) = 0 \tag{11}$$

$$\left.\frac{\partial\theta_2}{\partial y}\right|_{y=b_2} + \frac{Bi}{b_2}h(x)\,\theta_2(x,b_2) = \psi_2 b_2\left(1+\frac{Bi\,h(x)}{2}\right) \tag{12}$$

$$\left.\frac{\partial\theta_j}{\partial x}\right|_{x=0,a} = 0 \quad \text{for } j = 1,\ 2 \tag{13}$$

$$\theta_1(x,b_1) = \theta_2(x,0) \tag{14}$$

$$k_{1,y}\left.\frac{\partial\theta_1}{\partial y}\right|_{y=b_1} = k_2\left.\frac{\partial\theta_2}{\partial y}\right|_{y=0} \tag{15}$$

Using Fourier series expansion and separation of variables, the temperature solutions in layers 1 and 2 are found to be given by

$$\theta_1(x,y) = C_0\,y + \sum_{n=1}^{\infty} C_n\,\sinh(\lambda_n y)\cos(\lambda_n x) \tag{16}$$

$$\theta_2(x,y) = C_0\left(b_1+\frac{y}{\kappa}\right) + \sum_{n=1}^{\infty}\begin{pmatrix} C_n(\sinh(\lambda_n b_1)\cosh(\lambda_n y) \\ +(1/\kappa)\cosh(\lambda_n b_1)\sinh(\lambda_n y))\cos(\lambda_n x)\end{pmatrix} \tag{17}$$

where, $\lambda_n^2 = \beta_n^2\,(k_{j,y}/k_{j,x})$ and $\beta_n = n\pi/a$. Substituting Equation (17) in Equation (12) results in a linear system of N + 1 equations in N + 1 variables, namely C_0, C_1, $C_2 \cdots C_N$, where N is the number of eigenvalues considered in the solution. In order to determine these unknown coefficients, the principle of orthogonality is used, resulting in

$$C_0\left(\frac{a}{\kappa} + \left(\frac{Bi}{b_2}\right)\left(b_1+\frac{b_2}{\kappa}\right)\int_0^a h(x)\mathrm{d}x\right) + \sum_{n=1}^{\infty} C_n\left(\frac{Bi}{b_2}\right)P_n\int_0^a h(x)\cos(\lambda_n x)\mathrm{d}x = \int_0^a F(x)\mathrm{d}x \tag{18}$$

$$C_0\left(\frac{Bi}{b_2}\right)\left(b_1+\frac{b_2}{\kappa}\right)\int_0^a h(x)\cos(\lambda_i x)\mathrm{d}x + C_i\lambda_i\frac{S_i\,a}{2} + \sum_{n=1}^{\infty} C_n\left(\frac{Bi}{b_2}\right)P_n\int_0^a h(x)\cos(\lambda_n x)\cos(\lambda_i x)\mathrm{d}x = \int_0^a F(x)\cos(\lambda_i x)\mathrm{d}x \tag{19}$$

where,

$$S_n = \sinh(\lambda_n b_1)\sinh(\lambda_n b_2) + (1/\kappa)\cosh(\lambda_n b_1)\cosh(\lambda_n b_2) \tag{20}$$

$$P_n = \sinh(\lambda_n b_1)\cosh(\lambda_n b_2) + (1/\kappa)\cosh(\lambda_n b_1)\sinh(\lambda_n b_2) \tag{21}$$

$$F(x) = \psi_2 b_2\left(1+\frac{Bi\,h(x)}{2}\right) \tag{22}$$

Equations (18) and (19) are the result of the use of orthogonality principle to obtain a linear system of N + 1 equations in N + 1 variables. The index *i* in Equation (19) corresponds to the contribution of the diagonal terms of the matrix. Note that the standard approach of using principle of orthogonality for constant heat transfer coefficient results in explicit expressions for each unknown coefficient. However, similar to other papers addressing space-dependent convective heat transfer coefficient [18–20], in this case, since h is a function of x, a set of coupled, linear algebraic equations is obtained. The coefficients, C_0 and C_n's can be obtained by solving this set of linear algebraic equations. The final temperature solution in each layer is then given by substituting Equations (16) and (17) in Equation (9). The mathematical treatment for a slot jet on an infinite plate is the same, however, an appropriate length of the plate must be chosen during analysis.

2.2. Heat transfer due to a radial jet

The methodology for deriving the temperature distribution for a radial jet is similar to a slot jet, except that the cylindrical coordinate system must be employed. Further, because the effect of orthotropic thermal conduction in layer 1 is found to be negligible, as discussed in Section 3, the derivation in this section is presented for an isotropic insulation layer. Non-dimensionalization is first carried out using the following equations:

$$\begin{aligned} r^* &= \frac{r}{w};\ z^* = \frac{z}{w};\\ a^* &= \frac{a}{w};\\ b_1^* &= \frac{b_1}{w};\ b_2^* = \frac{b_2}{w};\\ T_j^* &= \frac{k_2\ (T_j - T_\infty)}{g_2\ w^2};\\ Bi &= \frac{h_{\max}b_2}{k_2};\ \psi_j = \begin{cases} 0 & j=1 \\ 1 & j=2 \end{cases} \end{aligned} \tag{23}$$

Similar to Section 2.1, the star (*) notation is dropped in the remainder of this section for convenience. In non-dimensional form, the temperature distribution is governed by

$$\frac{\partial^2 T_j}{\partial r^2} + \frac{1}{r}\frac{\partial T_j}{\partial r} + \frac{\partial^2 T_j}{\partial z^2} + \psi_j = 0\ ;\ \mathrm{j} = 1,\ 2 \tag{24}$$

subject to the following boundary conditions and interface conditions

$$T_1(r,0) = 0 \tag{25}$$

$$\left.\frac{\partial T_2}{\partial z}\right|_{z=b_2} + \frac{Bi}{b_2} h(r)\, T_2(r,b_2) = 0 \tag{26}$$

$$\left.\frac{\partial T_j}{\partial r}\right|_{r=0,a} = 0 \quad \text{for } j = 1,\ 2 \tag{27}$$

$$T_1(r,b_1) = T_2(r,0) \tag{28}$$

$$k_1 \left.\frac{\partial T_1}{\partial z}\right|_{z=b_1} = k_2 \left.\frac{\partial T_2}{\partial z}\right|_{z=0} \tag{29}$$

Equations (28) and (29) represent the compatibility condition at the interface where each layer is assigned its individual co-ordinate system with the origin at the bottom-left corner of each layer. Similar to previous section, a transformation is introduced in order to absorb the non-homogeneity in the governing Equation (24)

$$T_j(r,z) = \theta_j(r,z) - \frac{\psi_j}{2} z^2 \tag{30}$$

Based on the above transformation, the transformed boundary value problem is given by

$$\frac{\partial^2 \theta_j}{\partial r^2} + \frac{1}{r}\frac{\partial \theta_j}{\partial r} + \frac{\partial^2 \theta_j}{\partial z^2} = 0 \tag{31}$$

subject to the following boundary conditions and interface conditions

$$\theta_1(r,0) = 0 \tag{32}$$

$$\left.\frac{\partial \theta_2}{\partial z}\right|_{z=b_2} + \frac{Bi}{b_2} h(r)\, \theta_2(r,b_2) = \psi_2 b_2 \left(1 + \frac{Bi\, h(r)}{2}\right) \tag{33}$$

$$\left.\frac{\partial \theta_j}{\partial r}\right|_{r=0,a} = 0 \quad \text{for } j = 1,\ 2 \tag{34}$$

$$\theta_1(r,b_1) = \theta_2(r,0) \tag{35}$$

$$k_1 \left.\frac{\partial \theta_1}{\partial z}\right|_{z=b_1} = k_2 \left.\frac{\partial \theta_2}{\partial z}\right|_{z=0} \tag{36}$$

Following a similar procedure as Section 2.1, the temperature solutions in layers 1 and 2 are given by the following expressions

$$\theta_1(r,z) = C_0\, z + \sum_{n=1}^{\infty} C_n \sin h(\lambda_n z) J_0(\lambda_n r) \tag{37}$$

$$\theta_2(r,z) = C_0 \left(b_1 + \frac{z}{\kappa}\right) + \sum_{n=1}^{\infty} \begin{pmatrix} C_n(\sin h(\lambda_n b_1)\cos h(\lambda_n z) \\ +(1/\kappa)\cos h(\lambda_n b_1)\sin h(\lambda_n z))J_0(\lambda_n r) \end{pmatrix} \tag{38}$$

where λ_n's are roots of $J_1(\lambda_n a) = 0$. Substituting Equation (38) in Equation (33) results in a linear system of N + 1 equations in N + 1 variables. In order to determine the coefficients, the principle of orthogonality is used, resulting in the following set of algebraic equations in the unknown coefficients:

$$C_0 \left(\frac{a}{\kappa} + \left(\frac{Bi}{b_2}\right)\left(b_1 + \frac{b_2}{\kappa}\right) \int_0^a rh(r)\mathrm{d}r\right) + \sum_{n=1}^{\infty} C_n \left(\frac{Bi}{b_2}\right) P_n \int_0^a rh(r) J_0(\lambda_n r)\mathrm{d}r = \int_0^a rF(r)\mathrm{d}r \tag{39}$$

$$C_0 \left(\frac{Bi}{b_2}\right)\left(b_1 + \frac{b_2}{\kappa}\right) \int_0^a rh(r) J_0(\lambda_i r)\mathrm{d}r + C_i \lambda_i S_i N_{\lambda_i} + \sum_{n=1}^{\infty} C_n \left(\frac{Bi}{b_2}\right) P_n \int_0^a rh(r) J_0(\lambda_n r) J_0(\lambda_i r)\mathrm{d}r = \int_0^a rF(r)\cos(\lambda_i r)\mathrm{d}r \tag{40}$$

where,

$$N_{\lambda_i} = \frac{a^2}{2} J_0^2(\lambda_i a) \tag{41}$$

$$F(r) = \psi_2 b_2 \left(1 + \frac{Bi \cdot h(r)}{2}\right) \tag{42}$$

Equations (39)–(41) are the result of the use of orthogonality principle in radial systems to obtain a linear system of N + 1 equations in N + 1 variables. The index *i* in Equations (40) and (41) corresponds to the contribution of the diagonal terms of the matrix. In addition, Equation (41) represents the norm integral in radial systems [21]. Expressions for S_n and P_n are given by Equations (20) and (21) in Section 2.1. On solving the linear system of equations simultaneously, the coefficients C_0 and C_n's are determined, and thus, the temperature solution in each layer is given by substituting Equations (37) and (38) in Equation (30).

2.3. Heat flux correction factor

The heat flux correction factor needed to correctly account for lateral effects due to spatial variation in the heat transfer coefficient is defined as follows

$$\tilde{q}_c = \frac{(h_{\max} b_2/k_2)\cdot\varphi(x^*)\cdot T^*_{2,top}}{(b_2/w)^2} - 1 = \frac{Bi\cdot\varphi(x^*)\cdot T^*_{2,top}}{\left(b_2^*\right)^2} - 1 \tag{43}$$

Equation (43) is the dimensionless form of the heat flux correction factor, in which $T_{2,top}$ is $T_2(x, b_2)$ or $T_2(r, b_2)$ for Cartesian and cylindrical coordinate systems respectively. Note that the '*' notation has been adopted only for Equation (43) in this section. This is to distinguish between dimensional and dimensionless parameters in the general definition of the heat flux correction factor. In Equation (43), the function $(x^*) = h(x^*)/h_{max}$, $h(x^*) = h(x)$ since $x^* = x/w$ and the Biot number, *Bi* is defined as $h_{max}b_2/k_2$.

Note that when the heat transfer coefficient $h(x)$ is constant, the two terms in the numerator $h(x)\cdot(T_{2,top} - T_\infty)$ and $g_2 b_2$ are equal to each other based on overall energy conservation, and thus $\tilde{q}_c$ reduces to zero. When there is a spatial variation in h, Equation (43) accounts for the dimensionless correction factor in heat flux needed as a result. Note that this correction needs to be computed based on the temperature at the top of the two-layer structure, as

given by the final results of Sections 2.1 and 2.2 for slot and circular jets respectively.

For a fixed geometry and appropriate choice of thermal conductivity ratio, the heat flux correction factor $\tilde{q}_c$ is a function of three non-dimensional parameters – Bi, ρ and γ. While the theoretical models discussed above capture this dependence exactly, it is also desirable to determine simple power law correlations to represent these theoretical results. Such correlations could be used by experimentalists in the design of experiments and improvement in the accuracy of heat transfer measurements. The following section discusses results from this analysis.

3. Results and discussion

Fig. 4(a) illustrates the effects of lateral conduction for parameter values Bi = 0.001, ρ = 5 and γ = 2, for an infinite plate, i.e. for the case where the gradient region is far from any geometric boundaries. The peak positive and negative errors are labeled as e^+ and e^-. For a packet of thermal energy generated in the foil at a value of x just greater than 10, the path of least resistance is one that involves lateral conduction through the foil, and convection into the fluid at x < 10. The result is that around x = 10, the local wall-normal heat flux is no longer uniform, and increases above the nominally constant value for x < 10, and decreases for x > 10. In conventional methods of heat transfer measurements, this effect is not accounted for due to the one dimensional nature of the problem, whereas the two-dimensional analysis shown here accounts for this effect, resulting in greater accuracy.

For the case of a slot jet on a finite plate, Fig. 4(b) shows a comparison of the heat flux correction curves between an orthotropic insulation material and its isotropic equivalent for Bi = 0.001, ρ = 5, γ = 2 and κ = 1000 where κ = k_2/k_{1y} due to anisotropy and k_{1y} equals to k_1 for isotropic condition. Results indicate that there is not much variation in the correction factor for the case where the in-plane thermal conductivity is five times the out-of-plane thermal conductivity in the insulation material. For all subsequent results discussed in this section, both the resistive heater foil and insulation material are considered to have isotropic properties. In order to determine the number of eigenvalues required for accuracy of the temperature solution depend strongly on the values of ρ, γ and κ. Fig. 5 plots the residual as a function of x* along the y = b_2 boundary for the case ρ = 5, γ = 2 and κ = 1000. The residual is defined based on Equation (5) as the ratio of the heat flux at the heater foil boundary exposed to jet impingement to the effect of Newton cooling, in non-dimensional sense, $Bi\ h(x)\ T_2(x,b_2)/b_2$. The residual characterizes how well the solution satisfies Equation (5). Fig. 5 shows that as the number of eigenvalues increases, the residual approaches the ideal value of 1. Around 60 eigenvalues are needed for the residual to be nearly 1 over the entire range of x*. There may be significant error if a lower number of eigenvalues is used, particularly around $x^* = 1$ which represents the gradient region in the flow field.

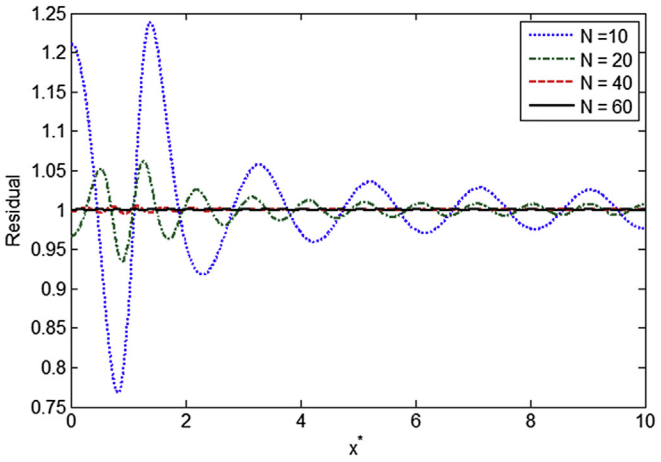

Fig. 5. Convergence in temperature solution as a function of maximum number of eigenvalues.

Fig. 6(a) and (b) illustrate the effect of foil to insulation thermal conductivity ratio, κ at varying Biot numbers for the case of a slot jet impinging on an infinite plate. Fig. 6(a) shows that for low foil-to-insulation conductivity ratio and a low value of Biot number, a large fraction of heat (≈40%) flows inward through the foil into the insulation, even for κ = 100. This is expected as the thermal resistance offered by the insulation material is lower than that offered by the impinging jet (i.e. $h_{min}b_1/k_1$ is O(1)). However, this is not desirable for experiments designed to calculate the heat transfer coefficient, as it leads to large $\tilde{q}_c$, and hence incorrect measurement of heat transfer. This can be improved by proper selection of foil and insulation materials such that ($h_{min}b_1/k_1 = Bi\ \beta\ \kappa/\rho \gg 1$), which is satisfied by selecting the conductivity ratio greater than 1000. For the same set of parameters and increased conductivity ratio, Fig. 6(b) shows improved results in terms of percentage errors. Regardless, the percentage error due to lateral

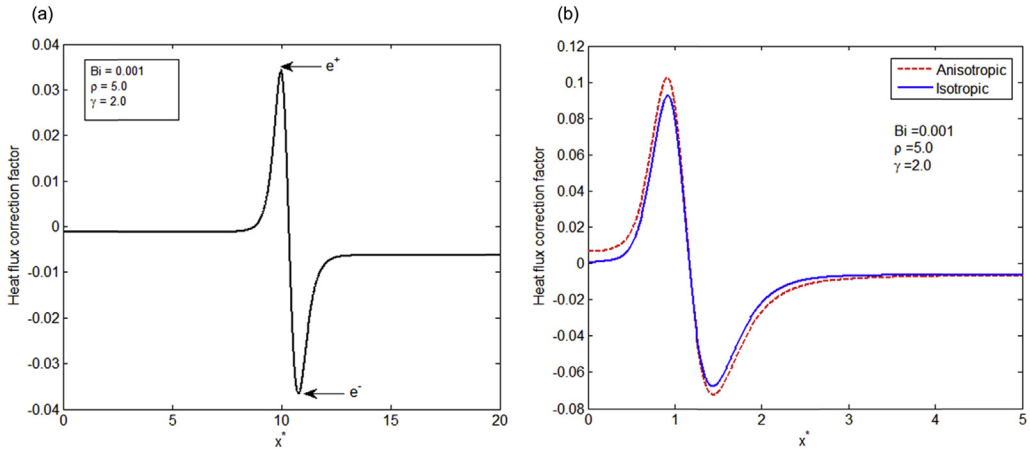

Fig. 4. (a) Heat flux correction curve illustrating lateral conduction effects for a slot jet over an infinite metal foil. (b) Comparison of finite plate heat flux correction curves for isotropic insulation layer with an orthotropic case, where in-plane thermal conductivity is five times the out-of-plane thermal conductivity.

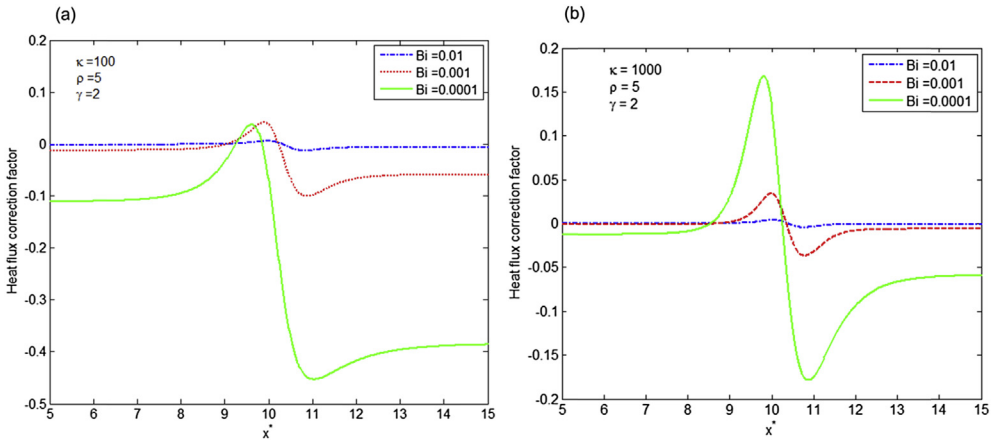

Fig. 6. Heat flux corrections for slot jet impingement over an infinite plate with $\rho = 5$ and $\gamma = 2$, for (a) $\kappa = 100$, (b) $\kappa = 1000$.

conduction effect is still large and can be further reduced by proper design of the experiments. For example, both Fig. 6(a) and (b) show significantly reduced error when the Biot number is large.

Similar results for slot jets are shown in Fig. 7(a) and (b) where the non-dimensional quantities, ρ and γ are varied at a constant Biot number of 0.001. These results indicate that as the ratio of maximum to minimum heat transfer coefficient increases, the resulting error increases, as expected. The parameter γ, as described earlier determines the gradient region of the jet. In Fig. 7(b) for $\gamma = 5$, the profile of the jet is that of a step, and maximum error in heat flux is observed. This is because due to sudden change in the jet profile, lateral effects are predominant as compared to the $\gamma = 0.5$ case, where the jet profile does not encounter an extreme step change. Most lab-scale experiments are analyzed by considering a symmetric profile for the jet. This is a reasonable approximation to make, however by forcing the symmetric condition, the percentage error increases as shown in Fig. 8. For instance, the peak error (e^+) in Fig. 8 is almost double of its infinite case equivalent Fig. 6(b) for a Biot number of 0.0001. The larger error primarily occurs due to the symmetric boundary condition forced on the side walls of the foil and insulation at $x = 0$. Fig. 9 illustrates the variation of ρ and γ for Biot number of 0.001 for a slot jet impinging on a finite length plate. Peak errors increase with increasing values of ρ and γ, as expected.

Fig. 10 illustrates the comparison between the errors for a radial jet impinging on a two layered disk for $\kappa = 1000$, $\rho = 5$ and $\gamma = 2$.

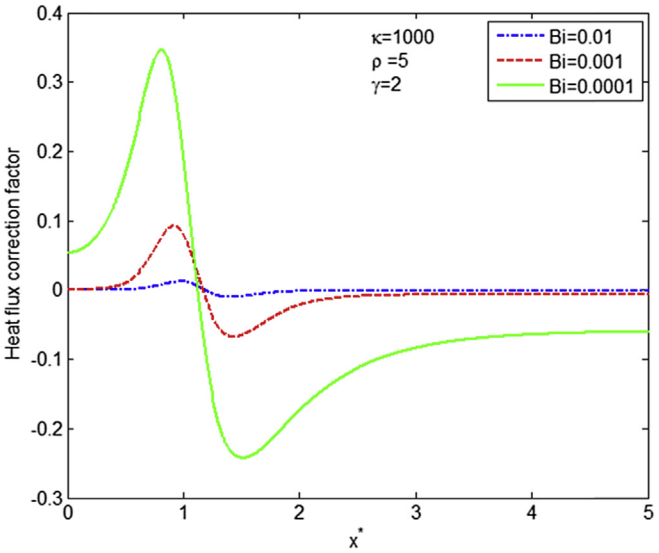

Fig. 8. Heat flux corrections for slot jet impingement over a finite plate with $\rho = 5$ and $\gamma = 2$, for $\kappa = 1000$.

The peak error (e^-) is appreciable for the Bi = 0.0001 case. Also in addition, with reduction in magnitude of the Biot number, the

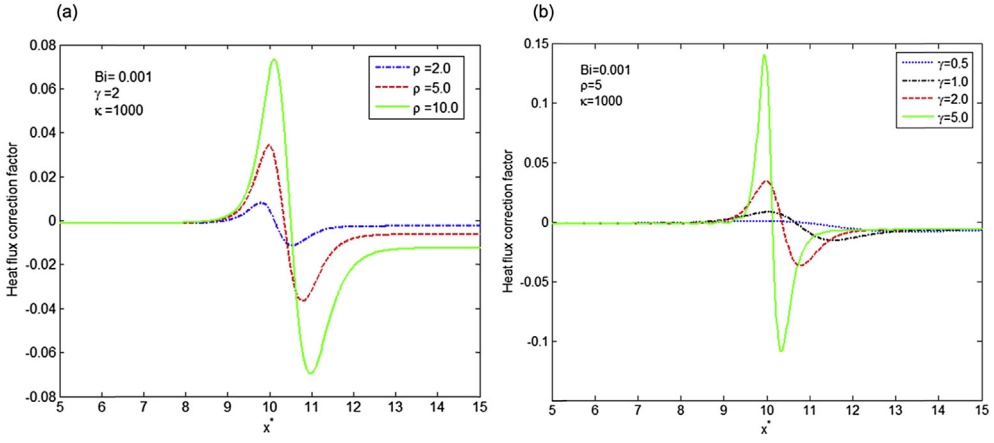

Fig. 7. Dependence of slot jet infinite plate heat flux corrections on (a) ρ, (b) γ ($\kappa = 1000$ and Bi = 0.001).

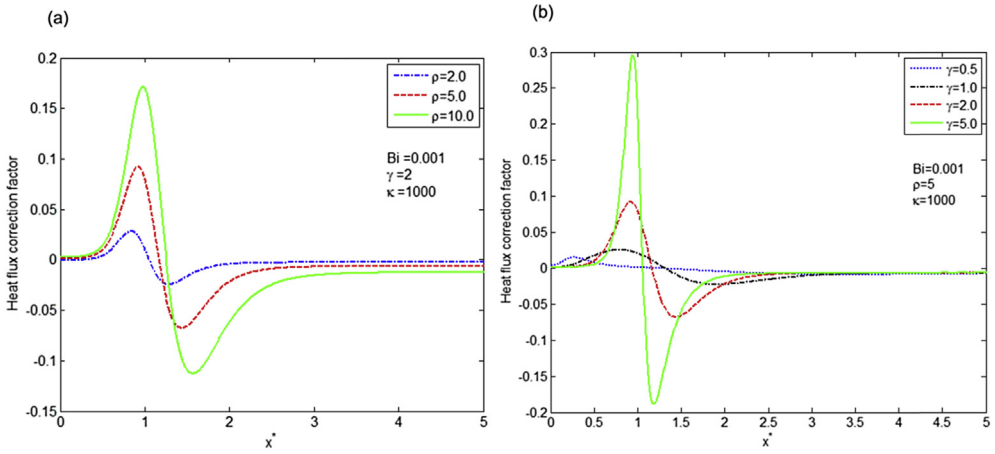

Fig. 9. Dependence of slot jet finite plate heat flux corrections on (a) ρ, (b) γ (κ = 1000, Bi = 0.001).

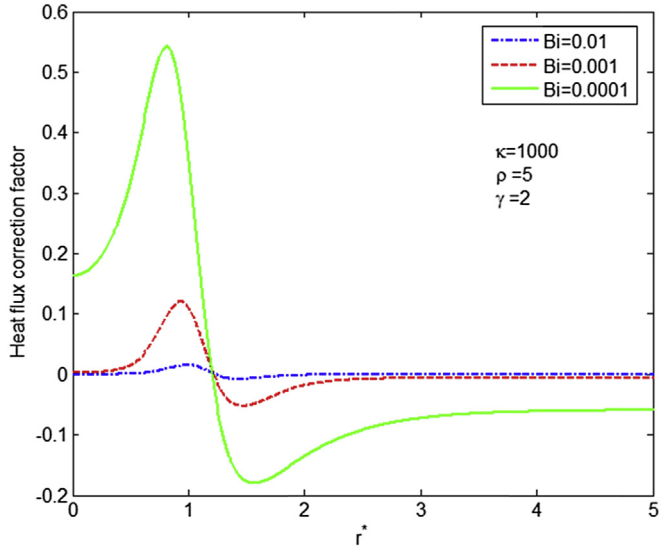

Fig. 10. Heat flux corrections for slot jet impingement over a disk with ρ = 5 and γ = 2, for κ = 1000.

conduction effects become predominant and hence the error increases. Fig. 11 illustrates the variation in the error for different values of ρ and γ while maintaining constant values for Bi and κ.

The mathematical analysis in Section 2 is used to calculate the correction factor and peak percentage errors for a wide range of test cases spanning the Bi, ρ and γ parameter space relevant for typical experimental conditions. Based on the results, correlations for estimating the percentage errors for all cases discussed in Section 2 are determined. These results may be useful to experimentalists in two ways, by both facilitating better experimental design and by allowing for corrections to measured data. For illustration, consider a heat transfer coefficient assumed to vary in the same manner as the Sherwood marked by inverted triangles on the aft portion of a turbine blade surface in Fig. 1. We stress that the actual data in Fig. 1 correspond to mass transfer measurements in which conduction errors are absent. In the non-dimensional coordinates used in the figure, the peak-to-base ratio of transport coefficient is 5, and occurs in the region $0.8 < S_p/C < 1.2$, with a maximum slope of about 12 (=γ) when the maximum value of Sh at $S_p/C = 1.4$ is normalized to unity. Using ρ = 5 and γ = 12, one can estimate measurement errors for a heat transfer measurement in the given situation. The ratio of thermal conductivity of heater foil to insulation (κ) rarely exceeds 100 in practice. Using these values, the experimentalist can use the correlations given in Figs. 11–13 to *a priori* estimate the error for a given Biot number, and thus adjust the dimensions of the heater foil and/or insulation thickness accordingly. This yields

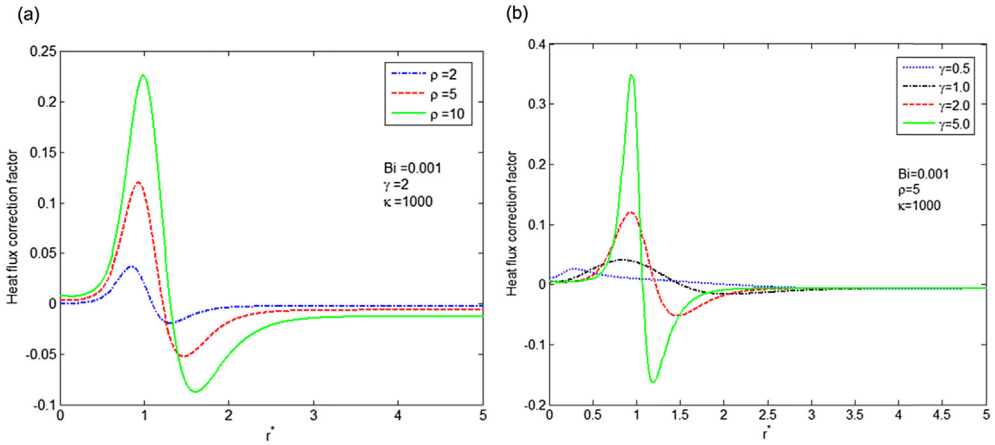

Fig. 11. Dependence of heat flux corrections for radial jet impinging on a disk on (a) ρ, (b) γ (κ = 1000, Bi = 0.001).

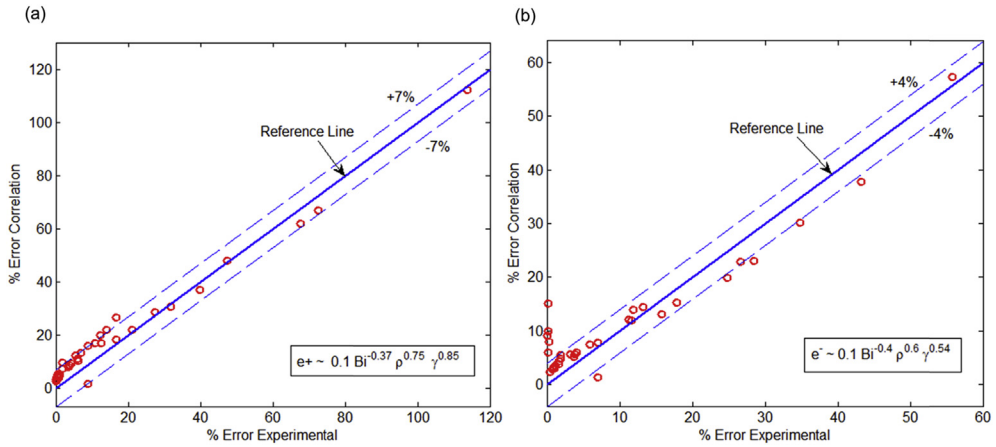

Fig. 12. Correlations for peak percentage error for infinite plate (a) positive error, (b) negative error.

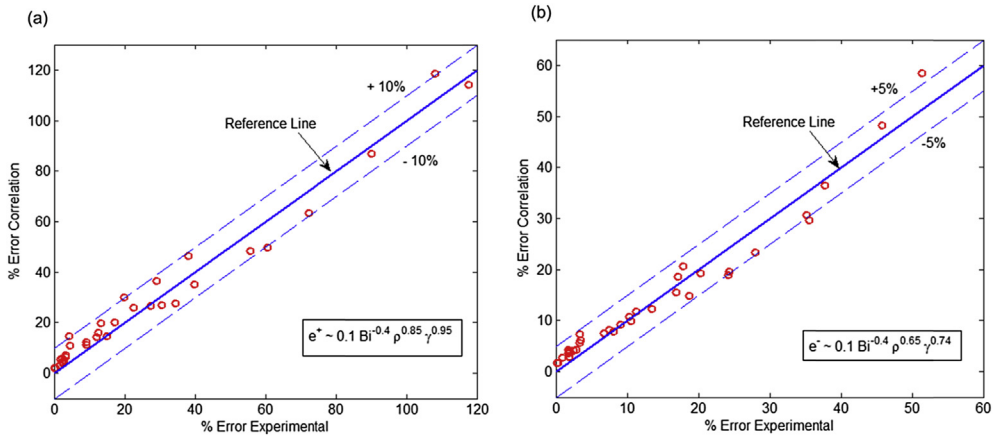

Fig. 13. Correlations for peak percentage error for finite plate (a) positive error, (b) negative error.

bounds on the maximum over- and under-estimation of the heat transfer coefficient in the vicinity of a gradient region. The correlations are, strictly speaking, valid only for the peak over- and under-estimate of the heat transfer coefficient, and do not give local corrections. However, one can observe that these maximum deviations occur at either end of the gradient region. Therefore, some information about the distribution can be obtained in the region where the errors are highest. To obtain a correction everywhere, one would have to repeat the analytical procedure presented in the paper. A power law expression is used to represent this data. The pre-factor and exponents in the power law are determined so as to minimize the least-squares error between the error predicted by the theoretical model and the power law. This procedure successfully provides correlations to accurately capture the theoretical

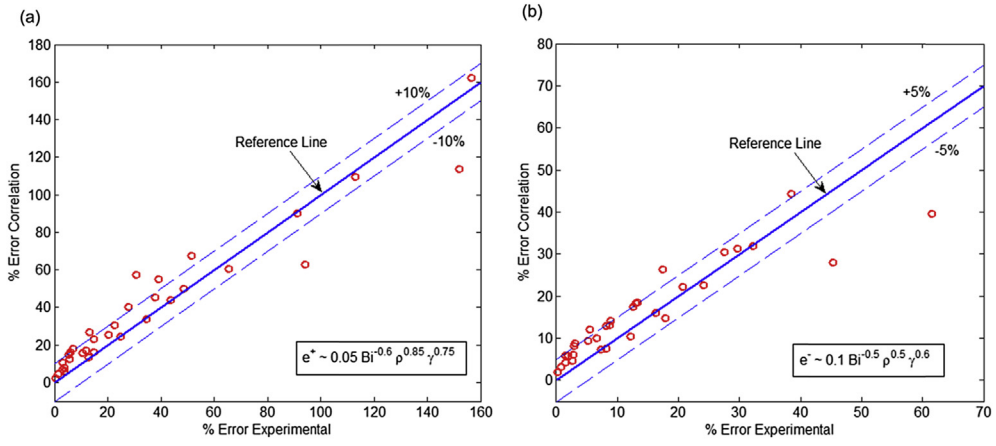

Fig. 14. Correlations for peak percentage error for disk (a) positive error, (b) negative error.

model results for each case. Fig. 12 presents the error from the theoretical model and from the power-law correlation for a slot jet impinging upon an infinite plate. The final form of the power law correlation is also shown. The ideal 45° line is shown. Subsequently, correlations with similar capabilities to represent results from the theoretical models are obtained for slot jets (finite plate) and circular jets (disk), are illustrated as Figs. 13 and 14. In each case, the correlation captures nearly all data within a 10% error band. This accuracy could be improved further by neglecting test cases corresponding to extremely poor experimental design.

4. Conclusion

A theoretical procedure to account for lateral thermal effects within a jet-cooled foil has been derived. The derivation provides a means for calculating a correction factor in the traditional heat transfer measurement methodology that accounts for two-dimensional nature of thermal transport due to spatial variation in the heat transfer coefficient. Since an impinging jet is known to present sharp gradients in the heat transfer coefficient, accounting for these effects is important. Analytical solutions for the temperature distribution are derived for both slot and circular jets for a foil with insulation material at the bottom. Results indicate that the correction factor is most sensitive and is inversely proportional to the Biot number, in addition to also being dependent on ρ and γ. Correlations are obtained for various experimental conditions that closely predict the peak errors obtained from the theoretical analysis. While the anisotropic nature of an insulating material is also accounted for in the theoretical model, results indicate that variation from the isotropic case is minimal. Results from this work may help improve the heat transfer measurements and design of equipment's that encounter sharp gradients in heat transfer due to external flow conditions.

Acknowledgements

Generous support from the Research Internship in Science and Engineering (RISE) Program of the Indo-US Science and Technology Forum and the Indian Institute of Science is gratefully acknowledged. Assistance from Ratnesh Raj in development of correlations is also gratefully acknowledged.

References

[1] Rose M. What should we measure? an aero-engine turbine aero-dynamic perspective. London, UK: Rolls-Royce plc; 1999. Technical Report No. RR-PNR-92620.
[2] Han JC, Dutta S, Ekkad S. Gas turbine heat transfer and cooling technology. CRC Press; 2012.
[3] Ekkad SV, Han JC. A transient liquid crystal thermography technique for gas turbine heat transfer measurements. Meas Sci Technol 2000;11(7):957.
[4] Goldstein RJ, Cho HH. A review of mass transfer measurements using naphthalene sublimation. Exp Therm Fluid Sci 1995;10(4):416–34.
[5] Ekkad SV, Ou S, Rivir RB. A transient infrared thermography method for simultaneous film cooling effectiveness and heat transfer coefficient measurements from a single test. In: ASME Turbo Expo 2004: power for land, sea, and air; 2004. p. 999–1005.
[6] Han S, Goldstein RJ. The heat/mass transfer analogy for a simulated turbine endwall. Int J Heat Mass Transf 2008;51(11):3227–44.
[7] Vedula RP, Metzger DE, Bickford WB. Effects of lateral and anisotropic conduction of local convection heat transfer characteristics with transient tests and surface coatings, 104; 1988. p. 21–8. Collected Papers in Heat Transfer, ASME, HTD.
[8] Lin M, Wang T. A transient liquid crystal method using a 3-D inverse transient conduction scheme. Int J Heat Mass Transf 2002;45(17):3491–501.
[9] Kingsley-Rowe JR, Lock GD, Owen JM. Transient heat transfer measurements using thermochromic liquid crystal: lateral-conduction error. Int J Heat Fluid Flow 2005;26(2):256–63.
[10] Bons J. Transient method for convective heat transfer measurement with lateral conduction—part I: application to a deposit-roughened gas turbine surface. J Heat Transf 2009;131(1):011301.
[11] Von Wolfersdorf J. Influence of lateral conduction due to flow temperature variations in transient heat transfer measurements. Int J Heat Mass Transf 2007;50(5):1122–7.
[12] Vogel G, Graf ABA, von Wolfersdorf J, Weigand B. A novel transient heater-foil technique for liquid crystal experiments on film-cooled surfaces. ASME J Turbomach 2003;125(3):529–37.
[13] Wang HP, Goldstein RJ, Olson SJ. Effect of high freestream turbulence with large length scale on blade heat/mass transfer. ASME J Turbomach 1999;121:217–24.
[14] Caciolli G, Facchini B, Picchi A, Tarchi L. Comparison between PSP and TLC steady state techniques for adiabatic effectiveness measurement on a multi-perforated plate. Exp Therm Fluid Sci 2013;48:122–33.
[15] Astarita T, Cardone G, de Luca L, Carlomagno GM. Some experimental investigations on gas turbine cooling performed with infrared thermography at Federico II. Int J Rotating Mach 2015;501:890414.
[16] Goldstein RJ, Behbahani AI, Heppelmann KK. Streamwise distribution of the recovery factor and the local heat transfer coefficient to an impinging circular air jet. Int J Heat Mass Transf 1986;29(8):1227–35.
[17] Siba EA, Ganesa-Pillai M, Harris KT, Haji-Sheikh A. Heat transfer in a high turbulence air jet impinging over a flat circular disk. J Heat Transf 2003;125(2):257–65.
[18] Sarkar D, Shah K, Haji-Sheikh A, Jain A. Analytical modeling of temperature distribution in an anisotropic cylinder with circumferentially-varying convective heat transfer. Int J Heat Mass Transf 2014;79:1027–33.
[19] Sarkar D, Haji-Sheikh A, Jain A. Thermal conduction in an orthotropic sphere with circumferentially varying convection heat transfer. Int J Heat Mass Transf 2015;96:406–12.
[20] Ma SW, Behbahani AI, Tsuei YG. Two-dimensional rectangular fin with variable heat transfer coefficient. Int J Heat Mass Transf 1991;34:79–85.
[21] Ozisik MN. Heat conduction. second ed. Wiley; 1980.